scientific reports

Check for updates

OPEN

Global proteomics reveals pathways of mesenchymal stem cells altered by *Mycobacterium tuberculosis*

Simran Kaur[1,3,4], Nupur Angrish[1,4], Madavan Vasudevan[2] & Garima Khare[1]✉

Mycobacterium tuberculosis (M. tb) **has a remarkable ability to persist inside host cells. Several studies showed that *M. tb* infects and survives inside bone marrow mesenchymal stem cells (BM-MSCs) escaping the host immune system. Here, we have identified various cellular pathways that are modulated in human BM-MSCs upon infection with virulent *M. tb* and the proteomic profile of these cells varies from that of avirulent *M. tb* infected cells. We found that virulent *M. tb* infection reshapes host pathways such as stem cell differentiation, alternative splicing, cytokine production, mitochondrial function etc., which might be modulated by *M. tb* to persist inside this unconventional niche of human BM-MSCs. Additionally, we observed that virulent *M. tb* infection suppresses various cellular processes. This study uncovers the differences in the host proteomic profiles resulting from the virulent versus avirulent *M. tb* infection that can pave the way to identify host-directed therapeutic targets for the treatment of tuberculosis.**

Keywords Host-directed therapeutics, Mesenchymal stem cells, Mycobacterium tuberculosis, Proteomics, Pathway analysis

In spite of the tremendous efforts, control of tuberculosis (TB) still remains a challenging task. Moreover, the onset of COVID-19 pandemic in 2020 has negatively impacted the progress made towards TB elimination in the past few years. According to WHO, in 2022, an estimated 10.6 million people fell ill with TB globally, out of which 1.3 million people died due to the disease[1]. Apart from this, one-fourth of the world's population is infected with dormant *M. tb*, which is at a lifetime risk of reactivation into active disease[1]. *M. tb* displays a remarkable tendency to modulate its active metabolic state to dormant state in the host and hides in various unconventional niches evading host immune surveillance, stressful environment as well as antibiotic treatment[2]. Therefore, in order to target these dormant bacteria, there is a need to understand the mechanisms of survival and persistence of dormant *M. tb* in such unconventional niches. One such niche is bone marrow mesenchymal stem cells (BM-MSCs), wherein bacteria can persist without getting eliminated by anti-TB drugs posing a threat for reactivation[3–10]. Our laboratory has previously demonstrated that *M. tb* when residing inside BM-MSCs was unresponsive to the action of anti-TB drugs as compared to when residing inside THP-1 macrophages, owing to the upregulation of host ABCG2 efflux pumps resulting in an enhanced efflux of the anti-TB drugs[11]. Since, *M. tb* and other pathogenic organisms are known to hijack host machinery and modulate the host cellular pathways for their own survival advantage, a detailed understanding of such mechanisms/pathways altered in hBM-MSCs by *M. tb* infection would help us to design novel strategies to target *M. tb* residing inside hBM-MSCs and eliminate this pathogen reservoir. Several studies have been conducted in macrophages where proteomics-based approach was employed for comprehensive study of the host proteome. Menon et al. have employed quantitative proteomics to understand the importance of lipid metabolism and host defence mechanisms in tackling bacterial infection[12]. Another study has showed that the exposure of mycobacterial cell wall lipids induces differential expression of several proteins in macrophages belonging to immune response, vesicle transport, oxidation and reduction and many more cellular processes[13]. These studies highlight the importance of proteomics-based strategies for the identification of various novel proteins and pathways that help in better understanding of host-pathogen interactions.

[1]Department of Biochemistry, University of Delhi South Campus, New Delhi 110021, India. [2]Genomics and Data Science Unit, Theomics International Pvt. Ltd, Bangalore 560038, India. [3]Children's Hospital of Eastern Ontario Research Institute, Ottawa, Canada. [4]These authors have contributed equally. ✉email: garimakhare@south.du.ac.in

In this study, we focused on identification of the changes induced by pathogenic *M. tb* in the proteome of human BM-MSCs to favour its own survival and further protect the pathogen from antibiotic assault and immune response by using global label-free proteomics approach. For this, to identify various proteins and pathways of hBM-MSCs that are modulated specifically with virulent *M. tb* infection, proteomics study was conducted with hBM-MSCs infected with the virulent as well as the avirulent *M. tb* strains. It is known that both *M. tb* H37Rv (virulent) and *M. tb* H37Ra (avirulent) are closely related strains of mycobacteria which differ mainly in their virulence potential[14]. Despite having equivalent MIC values for anti-TB drugs, these strains differ at their genetic and protein levels[15]. *M. tb* H37Ra bears a mutation in the *phoP* gene that encodes for a response regulator of the PhoP/PhoR two-component system. PhoP is essential for the virulence and is known to regulate several downstream genes including ESX-1 secretion system[16]. In the absence of ESX-1 secretion system, the pathogen is unable to release mycobacterial effector proteins into the host which might contribute to its avirulent nature. Moreover, it has been shown that *M. tb* H37Ra infects lungs and other organs with lower bacterial loads as compared to *M. tb* H37Rv, which fails to cause disease[17]. Apart from this, it has been previously demonstrated that infection with virulent or avirulent strain of *M. tb* invokes different expression profile in macrophages, suggesting the existence of different immunity mechanisms[18]. Uncovering the pathways that work differently in the virulent and avirulent infection highlights their importance in the host defence. and thus makes them potential targets for host-directed therapeutic approach for the elimination of the pathogen from the host.

Results

Propagation of hBM-MSCs

The hBM-MSCs were procured commercially and were successfully cultured and propagated. The cells achieved a confluency of ~80–90% in 6–7 days of revival and it was observed that passaging of the cells at less than 60–70% confluency resulted in extremely slow proliferation of the cells, thereby, suggesting the importance of cell-cell contact during expansion of hBM-MSCs in ex vivo culture. Figure 1 shows the images of the cells during propagation, wherein, long spindle-shaped and flattened cells were observed in the culture dishes, which is a characteristic morphological feature of the mesenchymal stem cells. Figure 1A represents cells observed at 3–4 days post culturing, whereas Fig. 1B, represents cells observed after 6–7 days post culturing. It was noted that

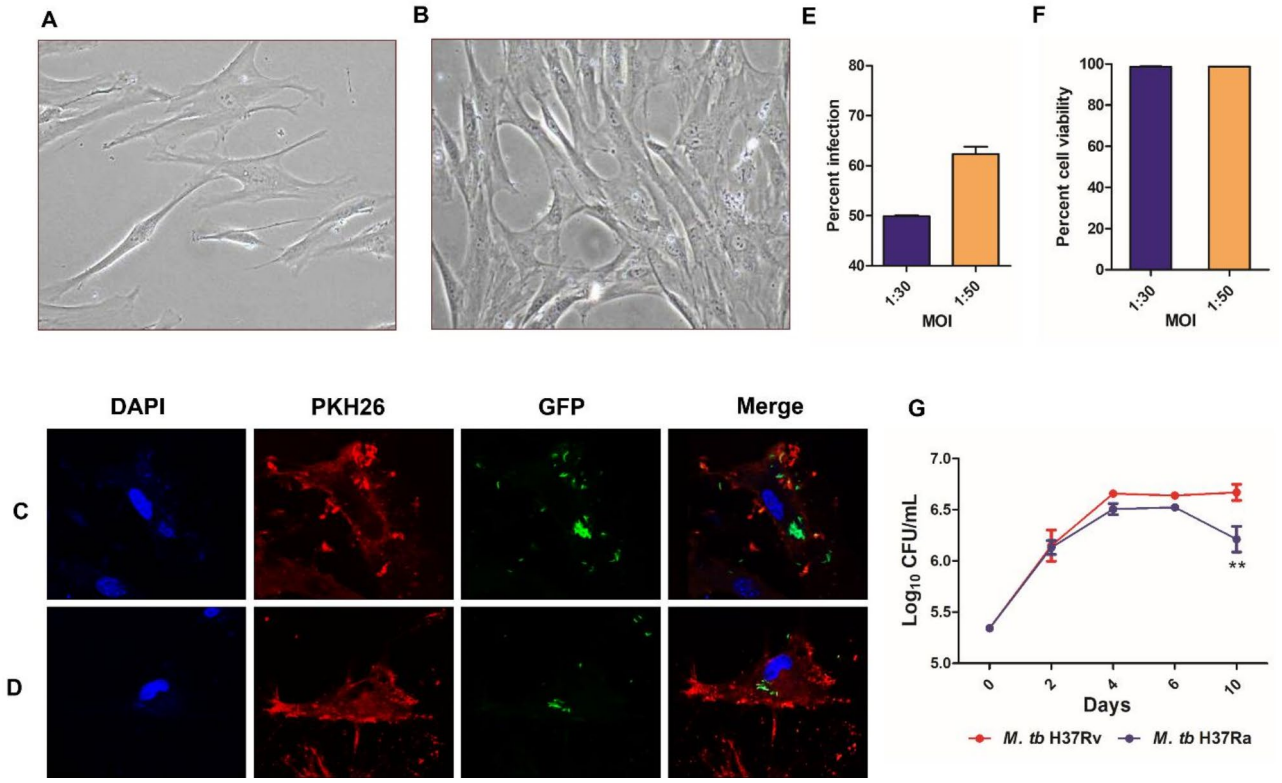

Fig. 1. Propagation of hBM-MSCs and their infection with *M. tb*. (**A**) Images of hBM-MSCs observed after 3–4 days post culturing. (**B**) Images of the cells observed after 6–7 days post culturing. Images were captured at 20X magnification. (**C**, **D**) Confocal microscopy representative images of hBM-MSCs (stained with PKH-26 dye) infected with *M. tb* H37Rv-GFP strain. The images were captured at 60X magnification. (**E**, **F**) Flow cytometric analysis of *M. tb* H37Rv-GFP infected hBM-MSCs at different multiplicity of infection (MOI) for percent infection and cell viability. (**G**) Growth Kinetics of *M. tb* H37Rv and *M. tb* H37Ra inside hBM-MSCs at various time points. The values are represented as the mean ± S.E.M of two independent experiments.

the cells grew in a healthy manner till passage 2, however, subsequently their growth rate was decreased. Hence, passage 2 cells were employed for all the studies.

Confocal microscopy of hBM-MSCs infected with *M. tb*

To verify the infection of cultured hBM-MSCs with *M. tb*, we performed confocal microscopy to visualize GFP expressing *M. tb* in hBM-MSCs after infection. Briefly, the cells were infected with *M. tb* H37Rv-GFP strain by employing the protocol described in the 'methods' section. The cells were fixed post infection and were stained with PKH26 dye and DAPI to label the cell membrane and the nucleus of the cells, respectively. It was observed that the bacteria were intracellularly localised inside hBM-MSCs as observed by GFP fluorescence in the cells (Fig. 1C,D). Thus, this confirmed the localisation of the *M. tb* inside hBM-MSCs and provided a validation for the infection protocol.

Virulent *M. tb* persists inside hBM-MSCs

In order to perform a global proteomics study of hBM-MSCs infected with *M. tb*, it was required that the sample for proteomics analysis comprised of a high number of *M. tb* infected viable cells. For this, we conducted a preliminary infection experiment wherein hBM-MSCs were infected with two different MOIs (1:30 and 1:50) and evaluated the percent infection of hBM-MSCs at each of the two MOIs. We observed that an infection with MOI of 1:50 resulted in ~62% infection without any significant loss of cellular viability, while an MOI of 1:30 led to ~49% infection (Fig. 1E,F). Since, the aim of the study was to identify the differential proteomic profile of BM-MSCs in response to infection, hence, the MOI of 1:50 for *M. tb* infection of hBM-MSCs for conducting proteomic study was selected. MSCs have been shown earlier to provide a protective niche to *M. tb*. It was shown that *M. tb* possesses the ability to survive and persist inside BM-MSCs by evading the immune surveillance and antibiotic treatment, however, the mechanisms responsible for the same are poorly understood. Therefore, we performed an untargeted global LC-MS/MS based proteomics which would reflect the dynamic state of the cellular proteome and will provide accurate overall protein signatures of a genome. Identifying various host proteins/pathways that are altered in hBM-MSCs by *M. tb* infection would help in bridging the gaps in the understanding of the mechanism(s) of pathogen's survival inside hBM-MSCs. Moreover, along with the virulent *M. tb* strain, we have also employed the avirulent *M. tb* H37Ra strain to specifically identify the proteins/pathways modulated inside hBM-MSCs upon infection with virulent *M. tb*. Towards this, a growth kinetic study was carried out for both the strains of *M. tb* i.e., virulent *M. tb* H37Rv and aviruent *M. tb* H37Ra, in order to determine the growth rates of these strains inside hBM-MSCs. It was observed that the virulent *M. tb* H37Rv strain was able to replicate inside hBM-MSCs till day 4 and thereafter, bacteria remained viable in a non-replicative manner albeit constantly maintaining the bacterial CFU. This observation corroborated with the earlier observation of *M. tb* reaching a dormant state in hBM-MSCs[3,10]. However, the avirulent *M. tb* H37Ra strain, replicated initially till day 4 inside hBM-MSCs with a subsequent decline in the bacterial CFU from day 6 onwards. At day 10, the avirulent strain exhibited ~0.5 log reduced CFU as compared to the virulent strain (Fig. 1G). Thus, the virulent *M. tb* is able to adapt more efficiently and remains dormant and in non-replicating state inside hBM-MSCs as compared to the avirulent *M. tb*, wherein, the host is able to combat the infection as observed by a decline in the CFU of avirulent *M. tb*. This differential ability of the host can be understood by global proteome profiling of virulent versus avirulent *M. tb* infected hBM-MSCs to delineate the mechanisms hijacked specifically by virulent *M. tb* for its own advantage and survival.

M. tb infection drives global cellular proteomic remodelling in hBM-MSCs

Figure 2A shows the design of the experimental protocol followed to conduct the proteomics study. We detected 2476 proteins in H37Rv infected hBM-MSCs lysate; whereas 2519 proteins were identified in H37Ra infected hBM-MSC lysate and a total of 2503 proteins were detected in uninfected control sample. This represented ~12.5% of the total human proteins that were detected in our investigation. Before further analysis, various statistical models were employed (2D-PCA and correlation matrix) in the study to determine the uniformity, robustness and reproducibility of the protein abundance levels obtained after MS (Fig. 2B–D)[19–21]. Downstream analysis of expressed proteome using amica showed significant reproducibility among the independent replicates. We observed varied global profiles in the protein data sets across different groups (*M. tb* H37Rv-infected, *M. tb* H37Ra-infected and uninfected hBM-MSCs) with less variation among the three independent replicates of a particular group (Fig. 2B,C). This suggested that the independent replicates were highly reproducible and the overall proteome of the hBM-MSCs altered significantly after infection as compared to uninfected state. As expected, we also observed that the virulent and avirulent strains of the bacteria evoke different protein expression outcomes in the host.

After establishing the reproducibility between the replicates, the proteomes of *M. tb* H37Rv-infected and *M. tb* H37Ra-infected hBM-MSCs were thoroughly analysed to determine the differentially expressed proteins (DEPs) induced as a result of bacterial infection. For this, three analysis groups were employed, namely, *M. tb* H37Rv-infected hBM-MSCs versus uninfected hBM-MSCs control (Rv Vs UI), *M. tb* H37Ra-infected hBM-MSCs versus uninfected hBM-MSCs control (Ra Vs UI) and *M. tb* H37Rv-infected hBM-MSCs versus *M. tb* H37Ra-infected hBM-MSCs (Rv Vs Ra) (Supplementary information S1). Critical evaluation of the differentially expressed proteins (DEPs) ($>\log2FC$, $pValue<0.05$) by visualizing the volcano plots and unsupervised hierarchical clusters showed notable and reproducible pattern of enriched and depleted proteins (Fig. 3). Volcano plots and Heat map analysis for comparison of the relative protein expression profiles amongst the three analysis groups reflected that the levels of majority of the host proteins altered upon virulent *M. tb* H37Rv infection in hBM-MSCs had decreased expression in comparison to the DEPs of hBM-MSCs infected with avirulent *M. tb* H37Ra strain (Fig. 3A–F; Table 1). In the Venn diagram-based distribution analysis of differentially expressed proteins (DEPs) among different groups, we found that a total of 200 proteins were

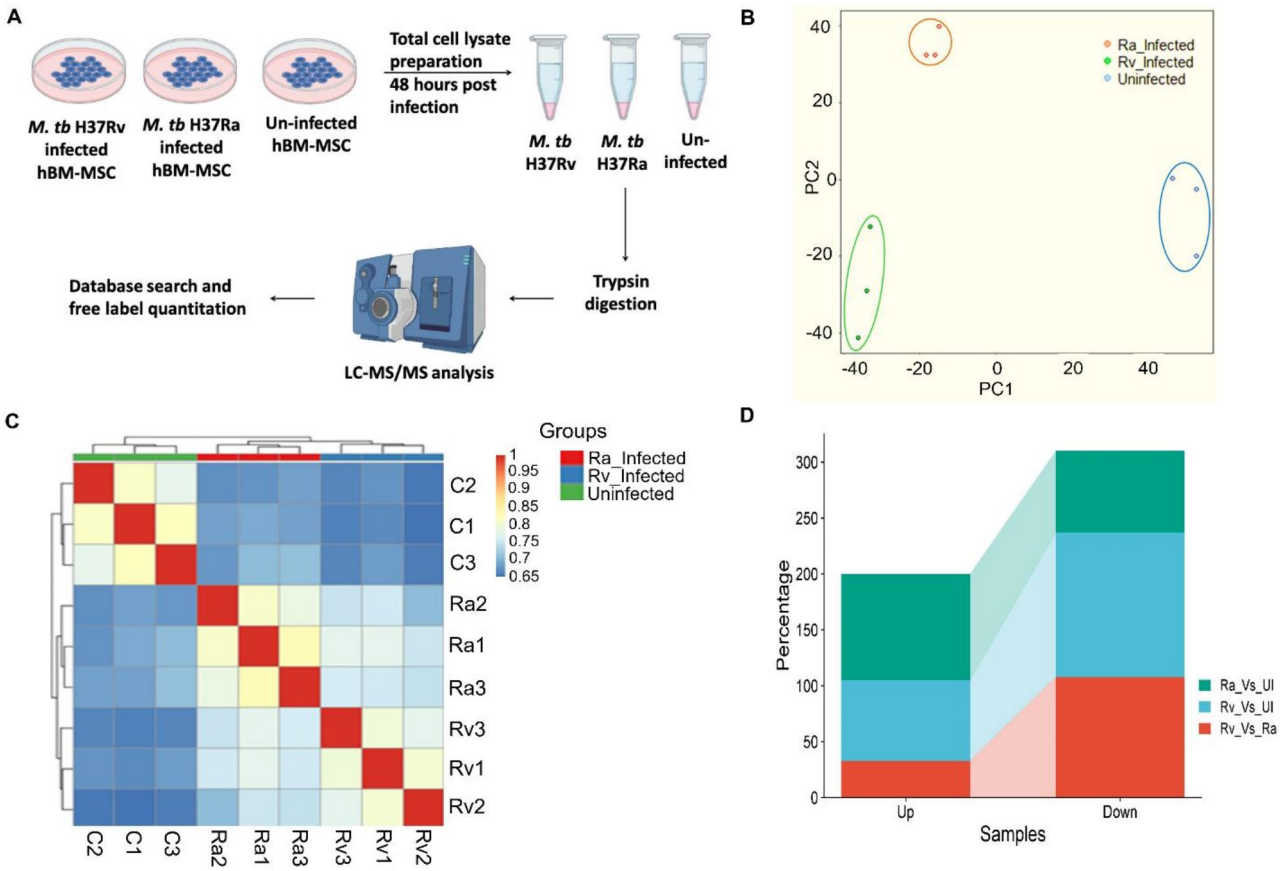

Fig. 2. Proteome profiling studies for *M. tb* infected hBM-MSCs. (**A**) Schematics representing the design of the experimental protocol of label free proteomics. hBM-MSCs were infected at an MOI of 1:50 with *M. tb* H37Rv and H37Ra strains. The proteins were extracted after 48 h of infection. After denaturation and trypsin digestion, samples were analysed using a Q Exactive hybrid quadrupole-orbitrap mass spectrometer. Mass spectrometry data were quantified by using Proteome discoverer 2.4. (**B**) Global proteome profiling of infected and uninfected hBM-MSCs shows significant reproducibility among the independent replicates as plotted by principle component analysis (PCA). (**C**) Replicate reproducibility was re-confirmed by the Pearson correlation coefficient based condition tree. (**D**) The proportional histogram represents the DEPs across the three analysis groups. Each comparison accounts for 100% of up and down regulated proteins and a total of 300% for three conditions is plotted in the Y axis. X axis represents up and down regulated proteins separately.

altered upon *M. tb* H37Rv infection as compared to uninfected hBM-MSCs, out of which 72 proteins were overexpressed and 128 proteins had decreased expression (Fig. 3G,H). However, in the case of *M. tb* H37Ra-infected hBM-MSCs versus uninfected group, 168 host proteins were found to be altered after infection with avirulent strain of bacteria. Out of these 168 proteins, there were 95 host proteins with increased expression and 73 proteins with decreased expression. Further, comparison of DEPs of *M. tb* H37Rv infected versus *M. tb* H37Ra infected hBM-MSCs led to the identification of 141 distinct host proteins whose expression levels were altered exclusively by virulent *M. tb* infection. Out of these, the expression levels of 33 proteins were increased and the levels of 108 proteins were decreased significantly in the hBM-MSCs. These results clearly indicate that the changes in protein profile after infection with virulent *M. tb* H37Rv strain as compared to avirulent and uninfected group, were more towards translational inhibition (downregulation of proteome) rather than increased synthesis (upregulation of proteome). Moreover, the Venn diagram depicts the intersection of various DEPs across these groups (Fig. 3G,H). Thus, these results suggested that virulent *M. tb* infection reshapes the host machinery and cellular pathways resulting in suppression of the levels of several proteins in order to survive inside the host BM-MSCs. There can be various mechanisms of reduction in protein levels such as activation of ubiquitin mediated protein degradation pathways, epigenetic modifications (histone modification and DNA methylation), regulation of expression by long non-coding RNAs or miRNA, manipulation of mRNA processing, changes in the mRNA stability and degradation etc., which would require further investigations[22].

Gene ontology (GO) and pathway analysis-insights into specific cellular changes in host upon infection

To elucidate the functional and biological relevance of the bacterial infection derived DEPs of hBM-MSCs, all the DEPs were subjected to identification of key gene ontology (GO) and pathways that were enriched harboring

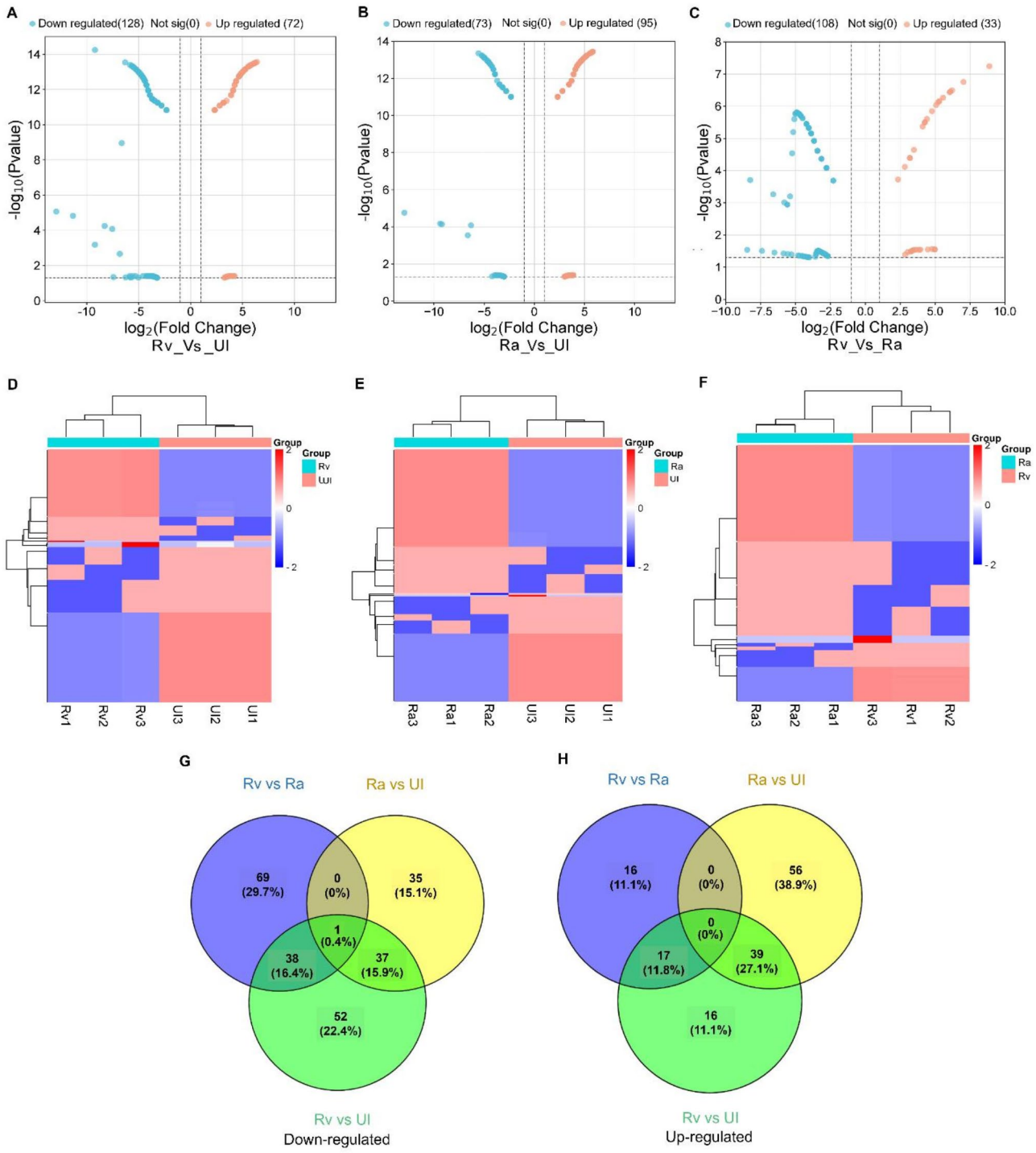

Fig. 3. Differential Proteome profiling of *M. tb* infected hBM-MSCs. (**A**–**C**) Volcano plot representation of enriched and depleted proteins in Rv infected in comparison to uninfected; Ra infected in comparison to uninfected and Rv infection in comparison to Ra infection. Enriched proteins are colored in red and depleted proteins are colored in blue. (**D**–**F**) Unsupervised hierarchical clustering of enriched and depleted proteins show clear and distinct pattern of enriched and depleted proteins in Rv infected in comparison to uninfected; Ra infected in comparison to uninfected and Rv infected in comparison to Ra infection. (**G**, **H**) Venn diagram-based representation of differential proteome revealed specifically enriched and specifically depleted proteins in each comparison group.

*Log2FC <-2 or > 2, $P < 0.05$.			
Groups	Total no. of differentially expressed proteins (DEPs)	No. of up-regulated proteins	No. of down-regulated proteins
Rv Vs UI	200	72	128
Ra Vs UI	168	95	73
Rv Vs Ra	141	33	108

Table 1. Differentially expressed protein of hBM-MSCs in response to *M. tb* H37Ra and *M. tb* H37Rv.

the DEPs in a statistically significant manner (Supplementary information S2). Clustering of enriched GO and pathways was performed and visualized as Balloon plot. A total of 19 GO and pathways were identified such as amino acid biosynthesis, calcium signaling, cell adhesion, cell adhesion and migration, collagen, extracellular matrix (ECM), host-pathogen interaction, immune response, lipoproteins, mitochondrial electron transport function, mitochondrial function, ROS response, proteases, protein ubiquitination, protein folding, vesicle trafficking, secretory protein transport, translation, and splicing (Fig. 4A,B). Moreover, it was observed that most of the altered proteins whether it showed increased or decreased expression in any of the infected groups, belonged to the pathways related to host-pathogen interactions, collagen/cell adhesion, immune response, mitochondrial function, lipoproteins, splicing/translation, and vesicle trafficking (Fig. 4A,B). On further analysis, we observed that in the case of avirulent *M. tb* H37Ra infected hBM-MSCs versus uninfected hBM-MSCs, proteins belonging to pathways such as ROS response, ubiquitin proteolysis pathway, mitochondrial electron transport function (bioenergetics) and lipoproteins were found to be enriched, whereas proteins of these pathways were either unchanged or exhibited decreased expression in the *M. tb* H37Rv infected cells versus uninfected cells (Fig. 4A,B). The enrichment of these specific pathway proteins in host hBM-MSCs infected with avirulent *M. tb* suggests their involvement in the host mechanisms to kill *M. tb* H37Ra, whereas, alterations in the levels of these proteins in the virulent *M. tb* infected hBM-MSCs, further substantiates that these proteins are required by the host cells to combat infection. In the case of analysis group virulent *M. tb* H37Rv infected hBM-MSCs versus uninfected, it was observed that proteins belonging to pathways related to vesicle trafficking, cell adhesion and migration, collagen, host-pathogen interactions, proteases, protein transport, and mitochondrial function were depleted, which were mostly unchanged in avirulent *M. tb* infected host cells, again pointing out to the fact that the virulent *M. tb* infection suppressed various pathways. This was interesting to note that there was an overall shutdown/suppression of the various key pathways by virulent *M. tb* infection that might act as a possible strategy contributing to the survival of the pathogen in the host cells and cause rewiring of these host immune-protective mechanisms for its own advantage. These enriched GO and pathways were considered as bridges and DEPs were considered as the nodes that connect the bridges. All the DEPs along with their biological role (GO and pathways) that was provided as input to RegNet algorithm (Theomics international Pvt. Ltd.) resulted in the modeling of protein: protein, protein: pathway, and protein: ontology along with the fold change and p-value (Student's t-test) for each of the DEP. The nodes were coloured according to their $\log_2$ ratios (abundance ratio) for each group. The bridge file output of the algorithm was visualized using Cytoscape v 2.8.3 to resolve the core protein network encompassing the DEPs like IL1B, COL1A1, CTGF, COL1A2, COL3A1, CXCL8, COL5A1, MMP14, MMP13, THBS2, COL12A1, CXCL1, LAMB1, APOE etc., that regulates host-pathogen interaction, immune response, collagen, ECM, cell adhesion and migration, and mitochondrial function (Fig. 4C–E).

The DEPs of pathways such as collagen, ECM, cell adhesion, proteases were strongly clustered and inter-related while host-pathogen interaction and immunity related DEPs formed another strong cluster. Most of the proteins found in 'Rv Vs UI' were altered as against their basal levels in uninfected cells suggesting that the proteome profile of hBM-MSCs was severely modulated by *M. tb* infection (Fig. 4C) while the same proteins were mostly unchanged in case of infection with avirulent *M. tb* H37Ra infection (Fig. 4D). Moreover, in the most critical network analysis group (Rv Vs Ra), the repressed protein nodes were of utmost importance because these proteins were suppressed in the host cells due to *M. tb* H37Rv infection, but were either unchanged or enriched in *M. tb* H37Ra infected hBM-MSCs (Fig. 4E). Therefore, they might represent the specific protein players involved in bacterial killing mechanism by the host. The pathways altered upon infection with virulent *M. tb* strain were further categorized into seven categories namely, RNA binding/alternate splicing, autophagy/vesicle fusion, ubiquinone synthesis/mitochondrial bioenergetics, metalloproteases, phagosome-endosome fusion, immune response related, and collagen/ECM/cell adhesion (Fig. 4F). Supplementary information S1 lists the DEPs associated with these pathways.

Thus, the proteins regulating these pathways offer a chance for further investigation to target virulent bacteria residing inside the hBM-MSCs.

Expression analysis for genes encoding DEPs

To experimentally validate the proteomics results, we performed real time PCR analysis. For this, 8 genes namely, *cxcl-10*, *mmp13*, *col1a2*, *clecb3*, *grem-1*, *uqcrh*, *gpx-1*, and *hnrnpk* were selected that belonged to five of the majorly altered pathways as given in Fig. 4F (immunity related pathways, metalloproteases, ECM/collagen/stemness related, mitochondrial bioenergetics and RNA binding/alternate splicing pathway). For the analysis, 1–2 genes were randomly selected from these pathways. For this, the total RNA was isolated from hBM-MSCs infected with virulent/avirulent *M. tb* strains/uninfected cells and was converted into cDNA by using the protocol mentioned in the 'methods' section. Real time PCR was conducted for each sample by employing gene specific primers (Table 2) followed by determination of ΔCt values after normalising the Ct values with

gapdh and further log2 fold change values were calculated by using ΔΔCt method (Fig. 4G,H). It was found that the mRNA levels of *cxcl-10*, *clecb3*, *mmp13* and *grem-1* were upregulated and the expression levels of *uqcrh*, *col1a2*, *gpx-1 and hnrnpk* were downregulated in virulent *M. tb* infected hBM-MSCs as compared to avirulent *M. tb* infected and uninfected cells (Fig. 4G,H). The observed fold changes in the mRNA levels of various genes in the virulent *M. tb* infected cells in comparison to avirulent infected cells were consistent with the protein abundance levels of these genes products in the proteomics results (Fig. 4H). Hence, these results substantiated our observations that infection with *M. tb* indeed alters the relative protein quantities in hBM-MSCs.

Discussion

Mycobacterium tuberculosis causes tuberculosis in humans and is one of the most successful pathogens. Its success lies in its ability to withstand the host mounted defences and to also undergo physiological adaptations by switching its metabolic state from active to latent state and vice-versa. Regardless of the presence of effective anti-TB drugs and a vaccine, *M. tb* continues to remain a global menace. Therefore, to fight the battle against this pathogen, designing of novel improved interventions is imperative.

BM-MSCs have been found as a niche for dormant *M. tb*[3]. However, the mechanism(s) by which the pathogen survives and persists inside these mesenchymal stem cells is poorly understood. Hence, knowledge of the key regulatory pathways/proteins of the host that are hijacked by *M. tb* post infection for its own persistence would be extremely useful in formulating novel approaches to kill these hidden bacteria and eliminate TB. Thus, in this study, changes in the proteomics profile of hBM-MSCs as a result of infection with virulent *M. tb* H37Rv/avirulent H37Ra strains was investigated by using a high throughput tandem MS-based proteomics approach. We demonstrated that unlike the virulent *M. tb*, avirulent strain of the bacteria is susceptible to host-mediated killing pathways and therefore, their viability starts to decline inside hBM-MSCs, however, the former strain continues to persist. This observation was in agreement with other studies, where the authors have demonstrated that the attenuated strain of *M. tb* gets killed by the action of cathelicidin inside BM-MSCs, whereas *M. tb* H37Rv could resist and therefore, was able to survive and persist inside these cells[7].

Further, we conducted a label-free MS-based proteomic analysis of *M. tb* H37Rv-infected, *M. tb* H37Ra-infected and uninfected hBM-MSCs, separately, where *M. tb* H37Ra-infected hBM-MSCs and uninfected cells were considered as reference controls for identifying *M. tb* H37Rv induced specific alterations in hBM-MSCs at the proteome level. It was found that the data generated by LC-MS/MS was reproducible (as assessed by 2D-PCA plot and correlation matrix) across all the three biological replicates of the 3 groups.

Various DEPs of hBM-MSCs were identified whose expression levels were altered upon *M. tb* infection as compared to uninfected control. Further, comparison of DEPs of *M. tb* H37Rv infected versus *M. tb* H37Ra infected hBM-MSCs led to the identification of 141 distinct host proteins whose expression levels were altered exclusively by virulent *M. tb* infection. Out of these, the expression levels of 33 proteins were increased and the levels of 108 proteins were decreased significantly in the hBM-MSCs. Enrichment analysis of GO and pathways harbouring differential proteome revealed that *M. tb* H37Rv infection when compared to *M. tb* H37Ra infection causes modulation of host proteins involved in major cellular processes such as RNA binding and splicing, immune response, mitochondrial function, vesicle trafficking, collagen related, ECM/cell adhesion etc. A very large complex network between DEPs was observed suggesting functional inter-connections between various pathways emphasizing on the overall reprogramming of several processes of hBM-MSCs by virulent *M. tb* for its survival and persistence.

Several studies have also demonstrated similar reprogramming and modulations of pathways in macrophage cells (primary host niche) after infection with *M. tb*. Various mechanistic strategies adopted by the pathogen have also been elucidated based on these studies conducted in infected macrophages such as, downregulation of autophagy, changes in cytoskeleton for pathogen's movement and dissemination in the host cell and alteration in the cytokine profile of macrophage resulting in reduced innate immune response[23–25].

Our study shows that *M. tb* can manipulate and modulate hBM-MSCs and some of the key pathways and proteins involved in the process are described below. It has been observed that the factors such as, EIF5B, EIF4G2, RPS27, RPS3, SRSF2, SRRM2, HNRNPK, and RNPS1 involved in RNA binding, translation, and splicing process showed significant depletion exclusively upon virulent *M. tb* infection. EIF4G2 and EIF5B are eukaryotic translation initiation factors that are known to dictate synthesis of proteins involved in various crucial processes[26]. A study showed that low-level of EIF5B is responsible for suppressed cell growth and proliferation and alters the cellular pathways associated with stress responses[27]. Similarly, EIF4G2 silencing also led to cellular growth inhibition, suppression of metastasis and tumorigenesis by inhibiting ERK signalling pathway in the case of hepatocellular carcinomas[28], signifying the importance of initiation factors in the cell proliferation. We also observed reduced levels of RNA binding factor RPS27, which is known to be associated with several biological processes such as proliferation, apoptosis, protein synthesis, alternate splicing[29,30]. Various investigators have shown the involvement of RPS27 in mediating innate immunity by activation of NF-κB signaling pathway[29,30]. RPS3, another ribosomal protein, that is induced by oxidative stress and bacterial infection has been shown to be involved in NF-κB mediated transcription of pro-inflammatory cytokines[31,32]. Hence, modulation in the expression levels of these proteins suggests that virulent *M. tb* targets ribosomal proteins to inhibit the host immune defence mechanisms, which is well suited for its survival in this niche. Alternative splicing is another crucial process that has been shown to be altered by various pathogens[33]. Infection of macrophages with virulent *M. tb* has been shown to affect alternate splicing resulting in various spliced or truncated versions of various genes[34]. We observed a decline in the levels of splicing proteins SRSF2 and SRRM2. The gene encoding for SRSF2 was also found to be downregulated in THP-1 macrophages after *M. tb* infection[35]. Penn et al. demonstrated physical interaction of splicing proteins including SRSF2 and SRRM2 with *M. tb* secreted protein Rv1827, highlighting a crucial role of host-pathogen interactions resulting in dynamic reprogramming of the host transcriptome[36].

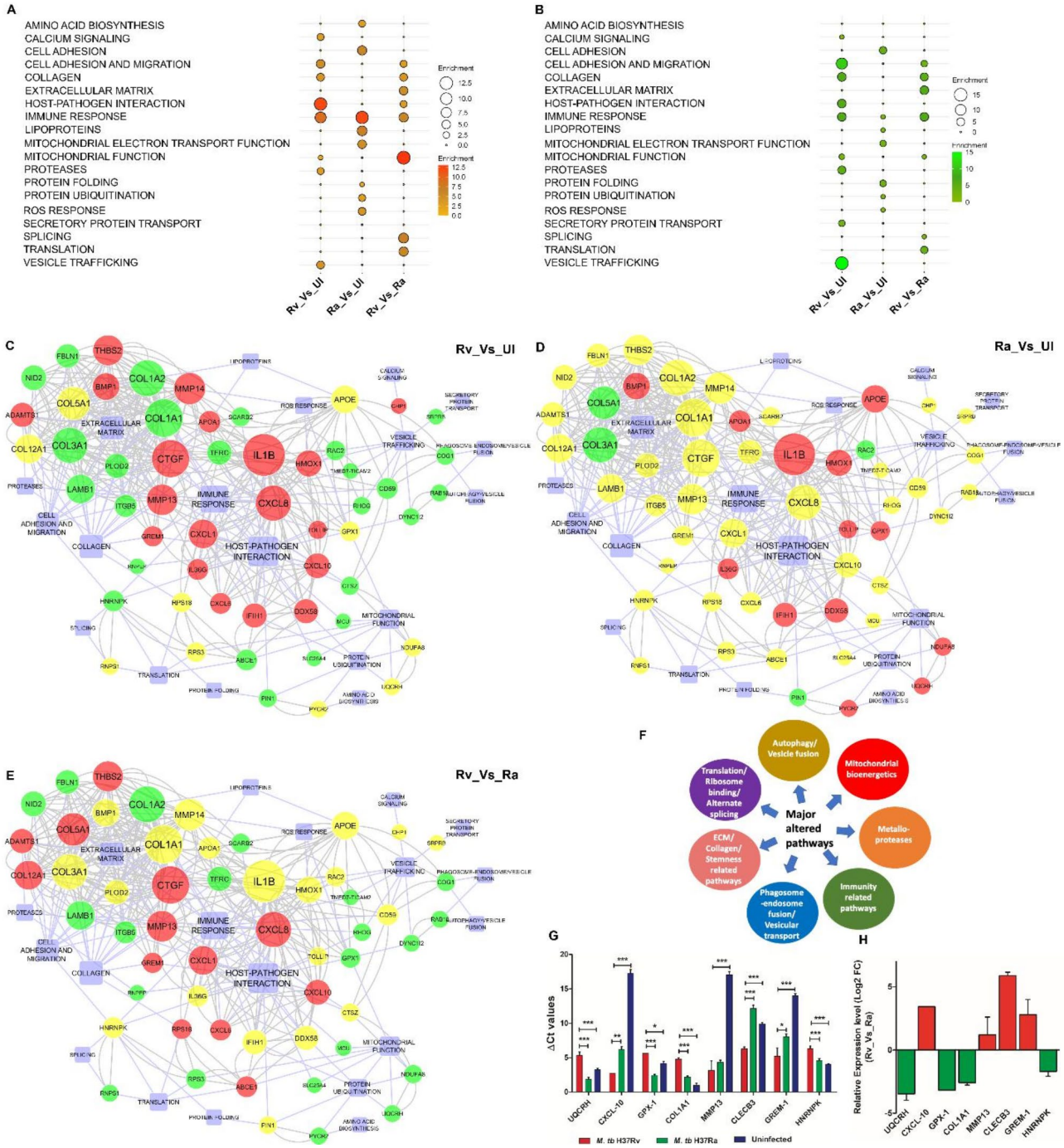

We also observed that several proteins involved in mitochondrial function and bioenergetics (UQCRH, NDUFA8, SLC25A11, SLC25A4, OXCT-1, GPX-1) were significantly decreased in virulent *M. tb* infected hBM-MSCs. In the case of macrophages infected with *M. tb*, a metabolic shift in the host energy metabolism is observed that is directly related to the cellular immune responses against the pathogen invasion[37,38]. However, it is known for stem cells that a reduction in oxidative phosphorylation and mitochondrial respiration has been linked with maintenance of their stemness properties and reduced differentiation abilities[39,40]. Thus, we believe that virulent *M. tb* drives hBM-MSCs towards a state of quiescence by maintaining stemness of the cells, reducing cell differentiation and proliferation pathways. Thus, decrease in the proteins involved in oxidative phosphorylation and ATP production appears to be useful for *M. tb* survival and evasion to keep this host cell niche in an undifferentiated quiescent state. However, further investigations will be required to validate this.

In addition to this, we observed that proteins belonging to ECM and collagen family (COL3A1, COL1A2, COL5A1, GREM-1, FBLN-1, THBS2, NID2) were highly altered upon *M. tb* infection. Previous studies have shown that during host infection, *M. tb* secretes factors that induce various host matrix metalloproteases to degrade ECM and collagen proteins and thereby, ensures their invasion and establishment of infection inside the cells[41,42]. Moreover, it has been known that in mesenchymal stem cells, collagen and ECM proteins regulate their differentiation and proliferation properties[43–45]. In our study, we observed that various collagen proteins

◀**Fig. 4**. Enrichment analysis of Gene ontology (GO) and pathways that harbour differential proteome. (**A**, **B**) Statistically significant and biologically relevant pathways that harbour differential proteome were visualized by using Balloon plot. GO and pathways harbouring list of enriched proteins (**A**) and depleted proteins (**B**) in each comparison group. (**C**–**E**) Statistically significant and biologically relevant pathways that harbour differential proteome upon network modelling resulted in key nodes (proteins & pathways) connected by edges (physical and binary Interaction). Color of the nodes indicate enrichment (red) depletion (green) and unchanged (yellow). Size of the nodes are proportional to the log fold enrichment or depletion score. Blue color square nodes indicate pathways. (**C**) Network profile of Rv infected in comparison to uninfected sample; (**D**) Network profile of Ra infected in comparison to Uninfected sample and (**E**) Network profile of Rv infection in comparison to Ra infection. (**F**) Pictorial representation of top pathways that are dysregulated upon infection as identified by comprehensive proteome profiling. (**G**) Real time PCR analysis of *M. tb* H37Rv infected hBM-MSCs, *M. tb* H37Ra infected hBM-MSCs and un-infected hBM-MSCs. GAPDH was used as an internal control to normalise the data and mRNA expression levels were compared across the samples by ΔCt values. Red, green and blue bars depict ΔCt values of *M. tb* H37Rv infected hBM-MSCs, *M. tb* H37Ra infected hBM-MSCs and un-infected hBM-MSCs, respectively. The experiment was conducted in triplicates. The data was analysed by one-way ANOVA, Tukey's multiple comparison test (*, $p < 0.05$; **, $p < 0.01$; ***, $p < 0.001$) by using GraphPad prism. (H) The bar diagram depicts relative expression level (log2 fold change) for various genes for the analysis group *M. tb* H37Rv infected hBM-MSCs vs. *M. tb* H37Ra infected hBM-MSCs. Red and green bars represent the genes that show upregulation and downregulation, respectively in the *M. tb* H37Rv infected hBM-MSCs in comparison to *M. tb* H37Ra infected hBM-MSCs.

Name	Forward primer (5′-3′)	Reverse Primer (5′-3′)
CXCL-10	CCACGTGTTGAGATCATTGC	TGCTCCCCTCTGGTTTTAAG
MMP-13	TTGAGCTGGACTCATTGTCG	GATTCCCGCGAGATTTGTAG
COL1A2	TTCTGCAACATGGAGACTGG	AATCCATCGGTCATGCTCTC
CLECB3	CCAGAAGCCCAAGAAGATTG	GGCTCTTGAGCTCCTCAAAC
GREM-1	CTTGGCCACCTCTCTTTTTG	ATGGGTGTGGCTTTTCTGAG
UQCRH	CGAGCAAAAGATGCTTACCG	CGGGCCTTTACACATTTCTC
GPX-1	CGCCAAGAACGAAGAGATTC	CTCGAAGAGCATGAAGTTGG
HNRNPK	AACGCCCTGCAGAAGATATG	GCCTCCTTTTCCAATCACTG

Table 2. List of the primer sequences employed for real time PCR study.

like COL3A1, COL1A2 were significantly reduced, whereas COL5A1 was enriched. These proteins are known to have a direct role in the differentiation of MSCs, as higher levels of COL3A1 and COL1A2 promote osteogenic differentiation of MSCs[46,47], whereas higher levels of COL5A1 inhibits osteogenic differentiation capacity of the multipotent stem cells[48]. Similarly, we observed high expression of GREM-1 (Gremlin-1) which is an antagonist of BMP (bone morphogenetic protein, involved in osteogenic differentiation of stem cells)[49]. GREM-1 has been demonstrated to inhibit osteogenic differentiation and senescence in stem cells[50]. Apart from this, we observed increase levels of thrombospondin (THBS2), which is known to inhibit osteogenic differentiation and MSCs proliferation[51–53]. Moreover, the levels of proteins such as filbulin-1 (FBLN-1) and nidogen-2 (NID2), that induces osteogenic differentiation, were also found to be reduced in our study[54–56]. Hence, the specific alterations in these proteins indicated a reduction in the differentiation of stem cells suggesting that the pathogen restricts the stem cells from differentiation and maintains their stemness, keeping them in an undifferentiated state that may be required for its own benefit to survive longer in this BM-MSC niche. However, a further detailed investigation into this phenomenon of *M. tb* survival will be required.

We also observed alterations in the proteins belonging to vesicular trafficking and protein transport. It has been previously demonstrated that autophagy can be an intrinsic mechanism for fusion of mycobacterial phagosome to lysosomes to kill intracellular *M. tb*[6]. Hence, reducing the autophagy and vesicular trafficking pathways could be a strategy for *M. tb* to persist in MSCs. Along the same lines, we observed a significant reduction in the expression of RAB5B and RAB5C, which are known regulatory GTPases and function in endocytic pathway of phagocytic cells[57,58]. Moreover, various dynein motor proteins involved in vesicle transport (DYNC1I2, DYNLL1) were also found to be decreased in hBM-MSCs upon *M. tb* infection. These proteins have been earlier shown to be involved in directing phagosomes towards lysosomes, and thus, are involved in promoting phagosome-lysosome fusion and pathogen killing[59]. Moreover, various proteins of vacuolar protein sorting complexes were found to be modulated by *M. tb* inside hBM-MSCs, such as VPS26A, VPS45, and VPS36. These are known to be involved in autophagy, cargo binding and selectivity and trafficking of vacuolar cargo[60–63]. Hence, downregulation of these proteins suggests that *M. tb* subverts the vesicular trafficking, autophagic response and protein transport for its survival.

Additionally, our data showed that proteins involved in immune responses such as CXCL-1, CXCL-6, CXCL-8 and CXCL-10, were increased upon *M. tb* infection in hBM-MSCs which is in accordance with the vital role of these pro-inflammatory cytokines in fighting against invading pathogens and attracting various immune cells like neutrophils, monocytes, T cells and B cells at the site of injury/inflammation[64]. Therefore, upregulation

of these cytokines involved in innate immune response can be directly correlated to the hBM-MSCs response towards bacterial antigens[65–68].

Taken together, our analysis revealed that *M. tb* modifies the host cellular dynamics extensively by altering key regulatory proteins and hijacking major functional pathways for its persistence and survival inside hBM-MSCs. Based on these results, we speculate that *M. tb* attempts to drive hBM-MSCs towards a state of quiescence by maintaining stemness of the cells, reducing cell differentiation and proliferation pathways; suppressing proteins involved in splicing and translation; and decreasing the intracellular vesicular trafficking and autophagy (Fig. 5). We believe that by modulating these host pathways, *M. tb* creates an inert environment for itself to thrive and perpetuate inside unconventional niche of hBM-MSCs. However, further investigations are needed to confirm these proposed strategies/mechanisms. This is the first study to report the proteomics profile of *M. tb* infected hBM-MSCs that compares changes in the abundance levels of proteins induced by virulent versus avirulent *M. tb* infection inside hBM-MSCs. Thus, this study has led to an increased understanding of the changes induced by pathogenic *M. tb* in the proteome of hBM-MSCs to favour its own survival, which paves the way for design and development of new host-directed therapeutic targets to kill this dormant population of *M. tb* from the host niches and prevent the problem of TB reactivation.

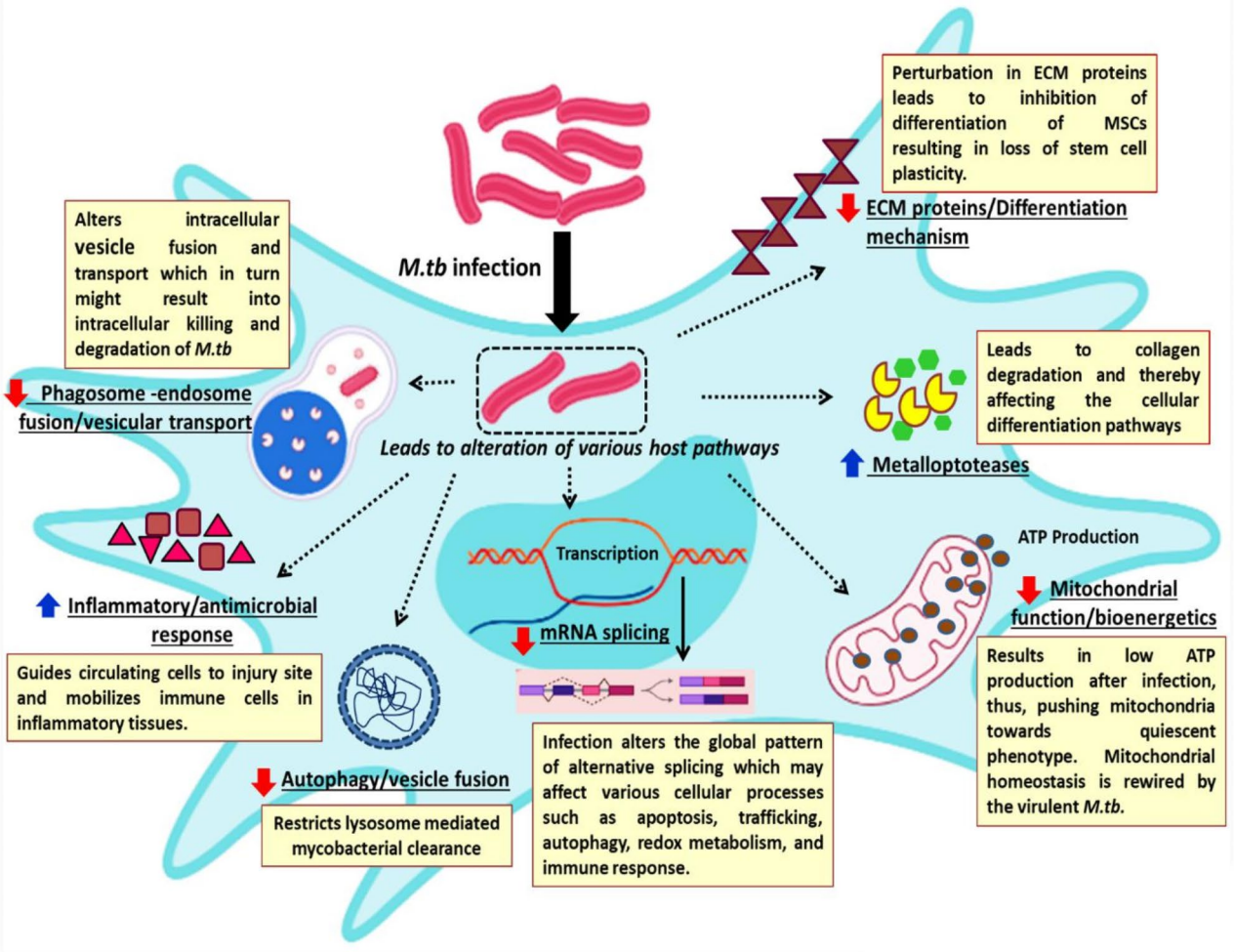

Fig. 5. The proposed model for alterations of host proteins/pathways of hBM-MSCs in response to *M. tb* infection: Exposure to *M. tb* triggers alterations of hBM-MSC proteome for its adaptation and longer survival inside the cell. Post invasion, pathogen modulates various key regulatory proteins of the host pathways and drives the cell towards quiescence by inhibiting various cellular differentiation and proliferation processes. *M. tb* also manages to suppress host defence pathways like phagosome-endosome fusion, autophagy, and apoptosis to prevent its clearance from the cell. Moreover, it interferes with the host alternative splicing machinery to affect several related processes/pathways like immune response, vesicular trafficking, and redox metabolism etc., by generating non-functional variants of important proteins. Not only it downregulates mitochondrial functioning but also rewires the mitochondrial ATP production to keep the cell arrested in quiescent state. Hence, in this way, *M. tb* resists various host mounted responses and continues to thrive inside the protective niche of hBM-MSCs. The red coloured downward arrows depict downregulation of the pathway and blue coloured upward arrows depict upregulation of the pathway in the cell.

Methods

Bacterial culture and growth conditions

M. tb strains (virulent *M. tb* H37Rv and avirulent *M. tb* H37Ra, obtained from All India Institute of Medical sciences (AIIMS), Delhi, India from Prof. Jaya Tyagi's lab) were grown in Middlebrook 7H9 broth medium (Becton Dickinson) supplemented with ADC (Albumin- Dextrose-Catalase) (Becton Dickinson), 0.5% glycerol and 0.2% Tween 80 with constant shaking at 200 rpm, 37 °C. Recombinant *M. tb* GFP strain was grown in the same conditions in the presence of 25 µg/ml kanamycin.

Culturing of cells

Human bone marrow mesenchymal stem cells (hBM-MSCs) were procured commercially from Thermo Fisher Scientific (catalog number-A15652) and were propagated in MesenPRO RS™ basal medium supplemented with MesenPRO RS™ growth supplement (Gibco, catalog number- 12746012). Briefly, the cells were revived by thawing a stock vial at 37 °C in a humidified 5% CO_2 incubator followed by addition of 1 ml supplemented media to the vial. The contents were transferred to a T-25 flask and incubated at 37 °C in a humidified 5% CO_2 incubator. After 24 h, the culture medium was replaced with fresh media and the cells were cultured for ~6–7 days till they reached a confluency of 70–80%. Further, the cells were split (ratio 1:2) in two T-25 flasks after trypsinization with 0.025% trypsin (CTS™ trypLE™ select enzyme, Thermo Fisher Scientific). The cells were propagated till passage 2 and then employed for conducting all the experiments.

Infection of hBM-MSCs with *M. tb*

The hBM-MSCs were infected with *M. tb* H37Rv-GFP expressing strain for confocal microscopy studies. hBM-MSCs were seeded on circular coverslips washed with 70% Ethanol and dulbecco's phosphate buffer saline (DPBS) and were incubated at 37 °C, 5% CO_2 for 16 h. A logarithmic phase culture of *M. tb* H37Rv-GFP cells was harvested, washed with 7H9 media, and employed for single cell preparation by using a previously published protocol[69]. Subsequently, the hBM-MSCs were infected with *M. tb* H37Rv-GFP bacteria at an multiplicity of infection (MOI) of 1:10 (hBM-MSCs: bacteria) for 8 h followed by amikacin (200 µg/ml) treatment for 1 h to remove the extracellular bacteria. The cells membrane were then stained with 2 µM PKH26 dye (Merck) for 15 min at room temperature (RT). The cells were then fixed with 4% paraformaldehyde (PFA) for 1 h followed by mounting of the coverslips onto the glass slides by using DAPI (4',6-diamidino-2-phenylindole) antifade stain (Invitrogen) followed by sealing of the coverslips. The cells were visualized by using Leica TCS SP8 confocal laser scanning microscope (Leica Microsystems).

Growth kinetics of *M. tb* inside hBM-MSCs

hBM-MSCs were infected with *M. tb* H37Rv (virulent) and *M. tb* H37Ra (avirulent) strains, separately at an MOI of 1:5 by using the protocol as mentioned above and incubated at 37 °C in 5% CO_2. The bacterial burden inside the cells was evaluated by CFU enumeration at various time points (day 0, 2, 4, 6, and 10). For this, the cells were lysed by the addition of 0.025% sodium dodecyl sulfate (SDS) solution for 15 min at 37 °C and the lysate was subjected to centrifugation at 12,000 rpm for 10 min at 4 °C. The supernatant was discarded and the pellet was resuspended in 100 µl 7H9 medium. Appropriate dilutions of the samples were plated onto 7H11 agar plates and the plates were incubated at 37 °C for 3–4 weeks.

Quantification of *M. tb* infection by using flow cytometry

The optimum MOI with highest percentage of infected cells was determined for conducting the proteomics study. Briefly, the hBM-MSCs were grown till passage 2 and seeded in a 6-well plate for overnight at a density of 2×10^5 cells/well. The cells were infected with *M. tb* H37Rv-GFP at different MOIs of 1:30 and 1:50 (hBM-MSCs: bacteria) by employing the protocol as mentioned above. After infection, the cells were retrieved, fixed by using 4% PFA solution for 30 min, and washed with DPBS for further evaluation by FACS for percent infection. The uninfected cells were employed to set voltages for forward scattering (FSC) and side scattering (SSC) in the plot. The infected cells were run at fluorescein iosothiocyanate (FITC) channel to obtain the values of percent infection. The cell viability was also checked by flow cytometer by using 7AAD staining which is a fluorescent marker for determining the cellular viability. For this, the cells were immediately mixed with 2 µl of the staining solution before acquisition in the flow cytometer. The cell counts were also determined by trypan blue staining.

Label free mass spectrometry based proteomics

The hBM-MSCs were seeded in a 6 well flat bottom plate at a density of 1×10^6 cells per well in triplicates (independent triplicates from 3 different passages of cells) and were infected with *M. tb* H37Rv and *M. tb* H37Ra cells, separately at an MOI of 1:50 (hBM-MSC: bacteria) for 48 h at 37 °C in a humidified 5% CO_2 atmosphere. After 48 h of infection, culture medium was aspirated from each well. Uninfected hBM-MSCs were employed as control. All wells were washed with 1 ml DPBS to remove any residual media components. The adherent cells were scraped and resuspended in G-buffer [0.1 M tris (pH 8.5) and 6 M guanidine hydrochloride] preheated at 70 °C, supplemented with 1X protease inhibitor cocktail (Roche). The lysed cell mixture was subjected to centrifugation at 14,000 rpm for 10 min at RT. The supernatant containing all the cellular proteins was collected, quantified and ~100 µg of protein sample was employed for proteome analysis. For performing mass spectrometry, proteins in the cell lysates were reduced with 20 mM dithiothreitol (DTT) and incubated at 95 °C for 10 min. Further, the sample was alkylated with 40 mM iodoacetamide in dark for 30 min to block free cysteine residues. The alkylation reaction was quenched by adding 10 mM DTT. Trypsin was added at a ratio of 1:50 (trypsin: lysate) and the samples were incubated at 37 °C overnight. Digested sample was cleaned by using a C18 silica cartridge column to remove the salt followed by drying using a speed vac vacuum concentrator at RT.

Peptides (~2 µg) from each sample were analyzed by reverse phase nano LC–MS/MS by using easy-nLC 1200 interfaced with a Q-exactive orbitrap mass spectrometer (Thermo Fisher Scientific). Samples were loaded onto a packed 75 cm x 50 cm PepMap RSLC C18 2 µm column (Thermo fisher scientific) by using mobile phase A (2% Acetonitrile + 98% water with 0.1% Formic acid) and mobile phase B (80% Acetonitrile + 20% water with 0.1% Formic acid). All samples were eluted from the analytical column at a flow rate of 300 nL/min by using a linear gradient of 5% solvent B to 45% solvent B over a duration of 104 min, followed by linear gradient of 45–90% of solvent B for 1 min. The column was regenerated by washing with 90% solvent B for 10 min and re-equilibrated with 5% solvent B for 3 min. Mass spectrometry data was acquired by using a data-dependent acquisition procedure and intact peptides were detected in the orbitrap at a resolution of 70,000 and a scan range of 350 − 2000 m/z. Peptides were selected for MS/MS and ion fragments were detected in the orbitrap at a resolution of 17,500 in a scan range of 200−2000 m/z.

Quantitative and qualitative identification of all the expressed proteins upon infection was performed using Proteome Discoverer 2.4 (Thermo Fisher Scientific). The output file with protein levels represented by Sequest HT along with its annotation from UNIPROT database (for *Homo sapiens*, 202,195 entries, October 2021) was subjected to normalization and differential proteome identification. Trypsin was employed as a protease with a maximum of two missed cleavage sites allowed. The mass tolerance for peptides was set to 10ppm and mass tolerance for fragment ions was set to 20mmu. Carbamidomethylation of cysteines was used as fixed modification, and oxidation of methionines, acetylation of lysine and histidine were used as variable modification. Peptides with only high confidence (target peptide FDR- 0.01) were used and minimum of one unique peptide was considered for successful protein identification. Quantitative proteomics analysis was carried out by using amica[70] web-based tool for quality control, differential expression, biological network and over-representation analysis. The replicate experiment data was analyzed for reproducibility by PCA and unsupervised correlation condition tree. Further, the differential proteome analysis was performed by comparing infected with uninfected proteome as well as Rv infected proteome with Ra infected proteome profiles. edgeR was used to perform DPA (differential proteome analysis) with a fold change of 2 and above with a FDR (false discovery rate) of pValue < 0.05. Unsupervised hierarchical clustering of DEPs was performed by using Cluster 3.0 and visualized using java tree view to identify the up and down-regulated protein clusters across the conditions compared. The DEPs were also visualized using volcano plot to understand the magnitude of change in protein expression as induction or repression.

The DEPs were further subjected to GO and pathway analysis using DAVID online tool with a FDR criterion of pValue < 0.05 to identify enriched pathways and gene ontology categories. SRPlot[71] was used to plot the DEP results for better understanding of the experimental changes. Statistically significant and biologically relevant gene ontology terms and pathways along with protein-protein interaction data of the DEPs were provided as input to RegNet al.gorithm (Theomics International Pvt. Ltd.). RegNet algorithm identifies the connecting nodes and edges from the raw input and derives the list of connections (gene-pathway-condition), enriched in the overall experiment. Further, this information was provided as an input to CytoScape V 2.8.2 (National Institute of General Medical Sciences by National Institutes of Health) to visualize the network. Force-directed spring-embedded layout algorithm was applied to the network and nodes were sized based on their connectivity score with larger nodes bearing the highest score.

Real-time PCR

Total RNA was isolated from all the three groups employed in the study (*M. tb* H37Rv infected hBM-MSCs, *M. tb* H37Ra infected hBM-MSCs and uninfected hBM-MSCs) by using Direct-zol RNA Miniprep kit (Zymo research) as per the manufacturer's protocol. Briefly, 1 ml TRIzol reagent (Invitrogen) was added into the wells to lyse the cells followed by loading of the entire lysate onto the RNA columns. The columns were washed by using RNA pre-wash and the samples were eluted from the columns in DNA/RNA-free water. The integrity of RNA was evaluated by using nano-drop machine. Total RNA (~2 µg) was converted to cDNA by using SuperScript IV VILO reverse transcription kit (Thermo Fisher Scientific) according to the manufacturer's protocol and gene specific primers for all the candidate genes were designed by using 'Primer 3' software (the primer sequences are mentioned in Table 2). Primers were procured (Merck) and the real time PCR reaction assays were performed in a total reaction volume of 10 µl by using PowerUp SYBR Green Master Mix (Applied Biosystems). The qPCR cycles were carried out under standard cycling conditions (stage 1: initial denaturation at 95 °C for 10 min, stage 2: consisting of 40 cycles of denaturation at 95 °C, for 15 s followed by annealing, extension and fluorescence reading at 60 °C for 1 min and stage 3: hold at 4 °C). The experiment was performed by using independent replicates. The gene expression in each group was normalized to GAPDH and the data is represented as ΔCt values. The differential expression was analyzed by using the ΔΔCt method and relative expression level (log2 fold change) of various genes was plotted.

Statistical significance

MS-based proteome analysis were performed for three groups (*M. tb* H37Rv infected hBM-MSCs, *M. tb* H37Ra cells infected hBM-MSCs and uninfected cells) separately in three independent replicates. The total of nine samples were processed and analyzed by a reverse phase nano LC–MS/MS by using easy-nLC 1200 interfaced with a Q-exactive orbitrap mass spectrometer. Further, qualitative and quantitative identification of all the expressed proteins was performed using Proteome Discoverer (version 2.0) and amica web-based tool. edgeR was used for differential proteome analysis, GO and pathway analysis was performed using DAVID online tool and protein-protein interaction was studied using RegNet algorithm. Statistical significance was performed by using Student's t test and a fold change of 2 and above with a false discovery rate of p Value < 0.05 was defined as cutoff in all analyses. The growth kinetics of *M. tb* H37Rv and *M. tb* H37Ra was analysed by plotting a graph

using GraphPad Prism. The data is represented as the mean ± SEM (error bars) of at least two independent experiments (*, $p < 0.05$; (**, $p < 0.01$; ***, $p < 0.001$, two-way ANOVA, Bonferroni post-tests).

Data availability

All the mass spectrometry raw data has been deposited at the ProteomeXchange consortium via the MassIVE partner repository (PXD050144). Data submitted to MassIVE (accession number- MSV000094167) can be accessed by using Username: MSV000094167_reviewer; Password- Gk.mtb123).

Received: 28 March 2024; Accepted: 8 October 2024
Published online: 28 December 2024

References

1. WHO global TB report. (2023). https://www.who.int/teams/global-tuberculosis-programme/tb-reports/global-tuberculosis-report-2023).
2. Upadhyay, S., Mittal, E. & Philips, J. A. Tuberculosis and the art of macrophage manipulation. *Pathogens Dis.* **76** (4), fty037 (2018).
3. Das, B. et al. CD271 + bone marrow mesenchymal stem cells may provide a niche for dormant Mycobacterium tuberculosis. *Sci. Transl. Med.*, *5*(170), pp.170ra13-170ra13. (2013).
4. Beamer, G., Major, S., Das, B. & Campos-Neto, A. Bone marrow mesenchymal stem cells provide an antibiotic-protective niche for persistent viable Mycobacterium tuberculosis that survive antibiotic treatment. *Am. J. Pathol.* **184** (12), 3170–3175 (2014).
5. Garhyan, J. et al. Preclinical and clinical evidence of Mycobacterium tuberculosis persistence in the hypoxic niche of bone marrow mesenchymal stem cells after therapy. *Am. J. Pathol.* **185** (7), 1924–1934 (2015).
6. Khan, A. et al. Mesenchymal stem cells internalize Mycobacterium tuberculosis through scavenger receptors and restrict bacterial growth through autophagy. *Sci. Rep.* **7**(1), 1–15 (2017).
7. Naik, S. K. et al. Mouse bone marrow Sca-1 + CD44 + mesenchymal stem cells kill avirulent mycobacteria but not Mycobacterium tuberculosis through modulation of cathelicidin expression via the p38 mitogen-activated protein kinase-dependent pathway. *Infect. Immun.*, *85*(10), pp.e00471-17. (2017).
8. Fatima, S. et al. Mycobacterium tuberculosis programs mesenchymal stem cells to establish dormancy and persistence. *J. Clin. Investig.* **130** (2), 655–661 (2020).
9. Jain, N. et al. Mesenchymal stem cells offer a drug-tolerant and immune-privileged niche to Mycobacterium tuberculosis. *Nat. Commun.*, **11**(1), 1–15 (2020).
10. Singh, V. K. et al. Human mesenchymal stem cell based intracellular dormancy model of Mycobacterium tuberculosis. *Microbes Infect.* **22** (9), 423–431 (2020).
11. Kaur, S., Angrish, N., Gupta, K., Tyagi, A. K. & Khare, G. Inhibition of ABCG2 efflux pumps renders the Mycobacterium tuberculosis hiding in mesenchymal stem cells responsive to antibiotic treatment. *Infect., Geneti. Evol.*, **87**, 104662. (2021).
12. Menon, D. et al. Quantitative lipid droplet proteomics reveals Mycobacterium tuberculosis induced alterations in macrophage response to infection. *ACS Infect. Dis.* **5**(4), 559–569 (2019).
13. Shui, W. et al. Quantitative proteomic profiling of host – pathogen interactions: the macrophage response to Mycobacterium tuberculosis lipids. *J. Proteome Res.* **8**(1), 282–289 (2009).
14. Zheng, H. et al. Genetic basis of virulence attenuation revealed by comparative genomic analysis of Mycobacterium tuberculosis strain H37Ra versus H37Rv. *PloS One*. **3** (6), e2375 (2008).
15. Heinrichs, M. T. et al. Mycobacterium tuberculosis Strains H37ra and H37rv have equivalent minimum inhibitory concentrations to most antituberculosis drugs. *Int. J. Mycobacteriol.*, **7**(2), p.156. (2018).
16. Forrellad, M. A. et al. Virulence factors of the Mycobacterium tuberculosis complex. *Virulence*. **4**(1), 3–66 (2013).
17. Li, H. et al. Quantitative proteomic analysis of host responses triggered by Mycobacterium tuberculosis infection in human macrophage cells. *Acta Biochimica et Biophysica Sinica*, **49**(9), pp.835–844 (2017) (a).
18. Li, P. et al. Comparative proteomics analysis of human macrophages infected with virulent Mycobacterium bovis. *Frontiers in cellular and infection microbiology*, **7**, 65 (2017) (b).
19. Friendly, M. Corrgrams: exploratory displays for correlation matrices. *Am. Stat.* **56**(4), 316–324 (2002).
20. Krummenauer, F. I: Boxplots-die flexible alternative zum „Antennenbildchen. *Klin. Monatsbl. Augenheilkd.* **219**(08), 613–615 (2002).
21. Patashnik, O., Lu, M., Bermano, A. H. & Cohen-Or, D. Temporal scatterplots. *Comput. Visual Media*. **6**(4), 385–400 (2020).
22. Denzer, L., Schroten, H. & Schwerk, C. From gene to protein—How bacterial virulence factors manipulate host gene expression during infection. *Int. J. Mole. Sci.*, *21*(10), 3730. (2020).
23. Maphasa, R. E., Meyer, M. & Dube, A. The macrophage response to Mycobacterium tuberculosis and opportunities for autophagy inducing nanomedicines for tuberculosis therapy. *Front. Cell. Infect. Microbiol.*, **10**, 618414. (2021).
24. Colonne, P. M., Winchell, C. G. & Voth, D. E. Hijacking host cell highways: manipulation of the host actin cytoskeleton by obligate intracellular bacterial pathogens. *Front. Cell. Infect. Microbiol.*, *6*, 107 (2016).
25. Mishra, M., Adhyapak, P., Dadhich, R. & Kapoor, S. Dynamic remodeling of the host cell membrane by virulent mycobacterial sulfoglycolipid-1. *Sci. Rep.* **9**(1), 1–13 (2019).
26. Lee, J. H. et al. Initiation factor eIF5B catalyzes second GTP-dependent step in eukaryotic translation initiation. *Proce. Natl. Acad. Sci.*, *99*(26), 16689–16694. (2002).
27. Jiang, X. et al. Proteomic analysis of eIF5B silencing-modulated proteostasis. *PloS One*. **11**(12), e0168387 (2016).
28. Li, S. et al. MiR-144-3p-mediated dysregulation of EIF4G2 contributes to the development of hepatocellular carcinoma through the ERK pathway. *J. Exp. Clin. Cancer Res.*, **40**(1), 1–14. (2021).
29. Diao, M. Q., Li, C., Xu, J. D., Zhao, X. F. & Wang, J. X. RPS27, a sORF-encoded polypeptide, functions antivirally by activating the NF-κB pathway and interacting with viral envelope proteins in shrimp. *Front. Immunol.*, **10**, 2763. (2019).
30. Wan, J., Lv, J., Wang, C. & Zhang, L. RPS27 selectively regulates the expression and alternative splicing of inflammatory and immune response genes in thyroid cancer cells. *Adv. Clin. Exp. Med.* **31**(8), 889–901 (2022).
31. Gao, X. et al. Bacterial effector binding to ribosomal protein s3 subverts NF-κB function. *PLoS Pathog.* **5**(12), e1000708 (2009).
32. Gao, X. & Hardwidge, P. R. Ribosomal protein s3: a multifunctional target of attaching/effacing bacterial pathogens. *Front. Microbiol.*, **2**, 137. (2011).
33. Chauhan, K., Kalam, H., Dutt, R. & Kumar, D. RNA splicing: A new paradigm in host–pathogen interactions. *J. Mol. Biol.* **431** (8), 1565–1575 (2019).
34. Kalam, H., Fontana, M. F. & Kumar, D. Alternate splicing of transcripts shape macrophage response to Mycobacterium tuberculosis infection. *PLoS Pathog.* **13**(3), e1006236 (2017).
35. Zhang, W., Niu, C., Fu, R. Y. & Peng, Z. Y. Mycobacterium tuberculosis H37Rv infection regulates alternative splicing in macrophages. *Bioengineered*. **9**(1), 203–208 (2018).
36. Penn, B. H. et al. An Mtb-human protein-protein interaction map identifies a switch between host antiviral and antibacterial responses. *Mol. Cell*. **71** (4), 637–648 (2018).

37. Kumar, R. et al. Immunometabolism of phagocytes during Mycobacterium tuberculosis infection. *Front. Mole. Biosci.*, 105. (2019).
38. Park, J. H., Shim, D., Kim, K. E. S., Lee, W. & Shin, S. J. Understanding metabolic regulation between host and pathogens: new opportunities for the development of improved therapeutic strategies against Mycobacterium tuberculosis infection. *Front. Cell. nfect. Microbiol.*, *11*, 635335. (2021).
39. Rigaud, V. O., Hoy, R., Mohsin, S. & Khan, M. Stem cell metabolism: Powering cell-based therapeutics. *Cells*, **9**(11), p.2490. (2020).
40. Buravkova, L. B. et al. Low ATP level is sufficient to maintain the uncommitted state of multipotent mesenchymal stem cells. *Biochim. et Biophys. Acta (BBA)-General Subj.* **1830**(10), 4418–4425 (2013).
41. Squeglia, F., Ruggiero, A. & Berisio, R. Collagen degradation in tuberculosis pathogenesis: the biochemical consequences of hosting an undesired guest. *Biochem. J.* **475**(19), 3123–3140 (2018).
42. Arbués, A., Schmidiger, S., Kammüller, M. & Portevin, D. Extracellular matrix-induced GM-CSF and hypoxia promote immune control of Mycobacterium tuberculosis in human in vitro granulomas. *Front. Immunol.*, *12*. (2021).
43. Gattazzo, F., Urciuolo, A. & Bonaldo, P. Extracellular matrix: a dynamic microenvironment for stem cell niche. *Biochim. et Biophys. Acta (BBA)-General Subj.* **1840**(8), 2506–2519 (2014).
44. Somaiah, C. et al. Collagen promotes higher adhesion, survival and proliferation of mesenchymal stem cells. *PloS One*. **10**(12), e0145068 (2015).
45. Novoseletskaya, E. et al. Mesenchymal stromal cell-produced components of extracellular matrix potentiate multipotent stem cell response to differentiation stimuli. *Fronti. Cell Dev. Biol.*, **8**, 555378. (2020).
46. Fernandes, H. et al. The role of collagen crosslinking in differentiation of human mesenchymal stem cells and MC3T3-E1 cells. *Tissue Eng. Part A*. **15**(12), 3857–3867 (2009).
47. Çelebi, B., Pineault, N. & Mantovani, D. The role of collagen type I on hematopoietic and mesenchymal stem cells expansion and differentiation. In *Advanced Materials Research* (Vol. 409, pp. 111–116). Trans Tech Publications Ltd. (2012).
48. Longo, A., Tobiasch, E. & Luparello, C. Type V collagen counteracts osteo-differentiation of human mesenchymal stem cells. *Biologicals*. **42**(5), 294–297 (2014).
49. Su, Z. et al. Overexpression of bone morphogenetic protein-1 promotes osteogenesis of bone marrow mesenchymal stem cells in vitro. *Med. Sci. Monit.: Int. Medi. J. Exp. Clin. Res.*, **26**, e920122-1. (2020).
50. Liu, H. et al. GREM1 inhibits osteogenic differentiation, senescence and BMP transcription of adipose-derived stem cells. *Connect. Tissue Res.* **62**(3), 325–336 (2021).
51. Jeong, S. Y. et al. Autocrine action of thrombospondin-2 determines the chondrogenic differentiation potential and suppresses hypertrophic maturation of human umbilical cord blood-derived mesenchymal stem cells. *Stem Cells*. **33**(11), 3291–3303 (2015).
52. Hankenson, K. D. & Bornstein, P. The secreted protein thrombospondin 2 is an autocrine inhibitor of marrow stromal cell proliferation. *J. Bone Miner. Res.* **17**(3), 415–425 (2002).
53. Jeong, S. Y. et al. Thrombospondin-2 secreted by human umbilical cord blood-derived mesenchymal stem cells promotes chondrogenic differentiation. *Stem Cells*. **31**(10), 2136–2148 (2013).
54. Cooley, M. A. et al. Fibulin-1 is required for bone formation and Bmp-2-mediated induction of Osterix. *Bone*. **69**, 30–38 (2014).
55. Hang Pham, L. B. et al. Investigating the effect of fibulin-1 on the differentiation of human nasal inferior turbinate-derived mesenchymal stem cells into osteoblasts. *J. Biomedical Mater. Res. Part. A*. **105**(8), 2291–2298 (2017).
56. Chen, Y. et al. Nidogen-2 is a novel endogenous ligand of LGR4 to inhibit vascular calcification. *Circul. Res.* **131**(12), 1037–1054 (2022).
57. Huang, H. et al. A dominant negative variant of RAB5B disrupts maturation of surfactant protein B and surfactant protein C. *Proc. Natl. Acad. Sci.* **119**(6), e2105228119 (2022).
58. Barbera, S. et al. The small GTPase Rab5c is a key regulator of trafficking of the CD93/Multimerin-2/β1 integrin complex in endothelial cell adhesion and migration. *Cell Commun. Signal.*, **17**(1), pp.1–15. (2019).
59. Rai, A. et al. Dynein clusters into lipid microdomains on phagosomes to drive rapid transport toward lysosomes. *Cell*. **164**(4), 722–734 (2016).
60. Roy, S. & Debnath, J. Autophagy enables retromer-dependent plasma membrane translocation of SLC2A1/GLUT1 to enhance glucose uptake. *Autophagy*. **13**(11), 2013–2014 (2017).
61. Zouhar, J., Rojo, E. & Bassham, D. C. AtVPS45 is a positive regulator of the SYP41/SYP61/VTI12 SNARE complex involved in trafficking of vacuolar cargo. *Plant Physiol.* **149**(4), 1668–1678 (2009).
62. Wang, R., Miao, G., Shen, J. L., Fortier, T. M. & Baehrecke, E. H. ESCRT dysfunction compromises endoplasmic reticulum maturation and autophagosome biogenesis in Drosophila. *Curr. Biol.* **32**(6), 1262–1274 (2022).
63. Garcia, E. J. et al. Membrane dynamics and protein targets of lipid droplet microautophagy during ER stress-induced proteostasis in the budding yeast, Saccharomyces cerevisiae. *Autophagy*. **17**(9), 2363–2383 (2021).
64. Kaufmann, S. H. Protection against Tuberculosis: cytokines, T cells, and macrophages. *Ann. Rheum. Dis.* **61**(suppl 2), ii54–ii58 (2002).
65. Monin, L. & Khader, S. A. December. Chemokines in Tuberculosis: the good, the bad and the ugly. In *Seminars in Immunology* (Vol. 26, No. 6, 552–558). Academic. (2014).
66. Domingo-Gonzalez, R., Prince, O., Cooper, A. & Khader, S. A. Cytokines and chemokines in Mycobacterium tuberculosis infection. *Tuberculosis and the tubercle bacillus*, pp.33–72. (2017).
67. Lombard, R. et al. IL-17RA in non-hematopoietic cells controls CXCL-1 and 5 critical to recruit neutrophils to the lung of mycobacteria-infected mice during the adaptive immune response. *PloS One*. **11**(2), 0149455 (2016).
68. Boro, M. & Balaji, K. N. CXCL1 and CXCL2 regulate NLRP3 inflammasome activation via G-protein–coupled receptor CXCR2. *J. Immunol.* **199**(5), 1660–1671 (2017).
69. Khare, G., Kumar, P. & Tyagi, A. K. Whole-cell screening-based identification of inhibitors against the intraphagosomal survival of Mycobacterium tuberculosis. *Antimicrob. Agents Chemother.* **57**(12), 6372–6377 (2013).
70. Didusch, S., Madern, M., Hartl, M. & Baccarini, M. amica: an interactive and user-friendly web-platform for the analysis of proteomics data. *BMC genomics*, *23*(1), 817. (2022).
71. Tang, D. et al. SRplot: a free online platform for data visualization and graphing. *Plos One*. **18**(11), e0294236 (2023).

Acknowledgements

We acknowledge BSL3 facility at the University of Delhi South Campus (UDSC), New Delhi, India for providing necessary facilities for conducting experiments related to the use of M. tb. We thank UDSC-CIF for the mass spectrometry and confocal services. We are also thankful to UDSC-Microarray facility and Prof. Amit Gupta for providing us generous access of equipment for conducting real-time PCR studies. We acknowledge Prof. Anil K. Tyagi and Dr. Prachi Nangpal for critical reading of the manuscript. We are thankful to Apoorva Mishra for providing help in preparation of the figures related to analysis of proteomics data.

Author contributions

S.K. and N.A. conducted the experiments. S.K. and N.A. analysed the data. M.V. analysed the proteomics data using bioinformatics. S.K. wrote the first draft of the manuscript. N.A. and G.K. wrote the final draft of the man-

uscript. G.K. conceived the study, provided overall supervision, and acquired funding for the study.

Funding
This study was financially supported by DU-IoE (Grant no. IoE-DU/MRP/2022/056), SERB, Department of Science and Technology, Government of India (CRG/2018/003325), UGC-SAP, and DU intramural funds. S.K. and N.A. received senior research fellowship from the Council of Scientific and Industrial Research, New Delhi, India.

Declarations

Competing interests
The authors declare no competing interests.

Additional information
Supplementary Information The online version contains supplementary material available at https://doi.org/10.1038/s41598-024-75722-5.

Correspondence and requests for materials should be addressed to G.K.

Reprints and permissions information is available at www.nature.com/reprints.

Publisher's note Springer Nature remains neutral with regard to jurisdictional claims in published maps and institutional affiliations.